LETTERS

Thermal lens effect for optimizing a passively Q-switched 1064 nm laser

Applied Physics Express **11**, 062702 (2018)
https://doi.org/**10.7567/APEX.11.062702**

Thermal lens effect for optimizing a passively Q-switched 1064 nm laser

Enbo Xing[1†], Jiamin Rong[2†], Si Ying Khew[1], Cunzhu Tong[3*], and Minghui Hong[1*]

[1]*Department of Electrical and Computer Engineering, National University of Singapore, Singapore 117576, Singapore*
[2]*Temasek Laboratories, Nanyang Technological University, Singapore 637553, Singapore*
[3]*State Key Laboratory of Luminescence and Applications, Changchun Institute of Optics, Fine Mechanics and Physics, Chinese Academy of Sciences, Changchun 130033, China*

*E-mail: tongcz@ciomp.ac.cn; elehmh@nus.edu.sg
†These authors contributed equally to this work.

Received March 11, 2018; accepted April 11, 2018; published online May 8, 2018

We demonstrate the improvement of pulse characteristics of a passively Q-switched laser by utilizing the thermal lens effect of a saturable absorber (SA) inside the cavity. The experimental results show that the SA should be considered as a convex lens inside the cavity, whose position strongly improves output performance. A fourfold enhancement of the average output power is obtained, and the peak energy increases from 8.2 to 25 μJ. Theoretically, we calculate the thermal lens effect of the SA and the optimal position inside the cavity, which agree with the experimental results.

End-pumped solid-state pulse lasers are attractive for many applications, such as target ranging, pollution monitoring, materials processing, and micromachining, and can provide a high peak power, short pulse width, high output beam quality, as well as other laser characteristics.[1–8] Recent advances have resulted in portable, compact, and low-cost laser devices.[9–14] However, for a continuous-wave pumping laser, there is the problem of thermal heat generation, which results in the reduction of efficiency, poorer cavity stability, and lower output beam quality.[15] There are two techniques commonly implemented to minimize the thermal effect: firstly, active cooling via air, water, and thermoelectric (TE) cooling systems; secondly, pulse laser-diode pumping to avoid thermal problems.[16–18] Although these methods address the issues of the thermal effect, the system requires a complex design, additional energy input, and a high cost.

Therefore, there is a significant need to manage the thermal effect. The thermal effect results in a thin equivalent lens forming within a laser crystal, which has been investigated by Song et al.,[15] Cousins,[19] and Neuenschwander et al.[20] In order to obtain a minimum beam inside a saturable absorber (SA) and thus achieve the lowest second Q-switching threshold, the SA is placed close to the output coupler due to the presence of a thermal lens effect (TLE) of the laser crystal.[21,22] In this case, the SA is perceived as a crystal without any optical functions. However, when oscillating light passes through the SA, the accumulation of heat in the SA should not be neglected.[23] In particular, for a high-peak-power-laser, it should be equivalent to a convex lens in the cavity, thus influencing the output performance strongly. Theoretically, it is possible to optimize output characteristics by taking advantage of the TLE, which affects the focal length and radius of curvature. The thermal effect of the SA is complex because the absorption coefficient α is dynamic and oscillating light is not continuous. There have been few studies on the influence of the TLE on the SA inside the cavity.[23,24]

In this paper, an equivalent model is proposed, in which a laser crystal and SA crystal are represented by two optical lenses, to investigate the effect of the TLE on the position of the SA to improve pulse laser performance. The experimental results demonstrate that an optimal position exists that gives the highest average output power. A slope efficiency of 29.5% is obtained, with about 4 times improvement of the average output power and about 3 times improvement of the peak energy. Theoretically, the TLE is calculated at different positions inside the cavity. These calculations are in agreement with experimental measurements, showing a strong correlation between the optimal position and pump power, which can be explained by the TLE.

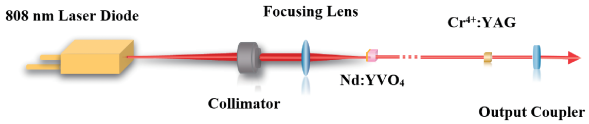

Fig. 1. Schematic of the passively Q-switched diode-pumped Nd:YVO_4 laser setup.

Figure 1 presents the schematic of the experimental setup for the laser-diode-pumped passively Q-switched laser. The gain medium is a plane-parallel 5-mm-long *a*-axis-cut Nd:YVO_4 crystal doped with 0.5 at. % Nd^{3+} ions. The pump surface is coated for high reflectivity (HR, $R > 99.9\%$) at 1064 nm and high transmissivity (HT, $T > 99.7\%$) at 808 nm, which is used as the input mirror (M_1); the opposite surface is coated for HT ($T > 99.8\%$) at 1064 nm. The SA used is a 1.5-mm-length [100]-cut Cr^{4+}:YAG crystal with initial transmission (T_0) of 75%. Both surfaces of the Cr^{4+}:YAG crystal are coated for antireflection (AR, $R < 0.2\%$) at 1064 nm. The laser crystal and SA are mounted onto aluminum holders with a diameter of 3 mm and operate at room temperature. A flat mirror with reflection of 90% at 1064 nm is used as an output coupler (M_2). The pump source is a fiber-coupled 808 nm laser diode (Focuslight FL-FCSE08-7-808-200-0.22) with a core diameter of 200 μm and numerical aperture of 0.22. In order to achieve a suitable wavelength for maximum absorption of the laser crystal, a TE cooler is used to adjust the operation temperature for the laser diode. A collimator (Thorlabs F220SMA-780) and a focus lens coated with a 808 nm AR coating (Newport PAC03AR) are used to focus the pump beam into the Nd:YVO_4 crystal. To provide a stronger TLE, the diameter of the pump spot is only 150 μm. The average output power (Newport 2935-C) and pulse characteristics (Tektronix TDS714L) are measured. The thermal lens focal length is usually on the order of 10 cm; hence, the cavity length is specified at 15.5 cm to investigate the effect of the thermal lens on the output performance.

The average output power versus pump power at different positions of the SA in the cavity is shown in Fig. 2. In order

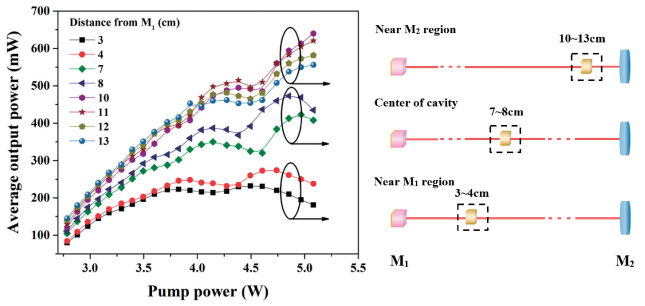

Fig. 2. Average output power versus pump power at different distances from M_1. These power curves are divided into three regions, the near-M_1 region (the distances from M_1 are 3–4 cm), the center of the cavity (7–8 cm from M_1), and the near-M_2 region (10–13 cm from M_1).

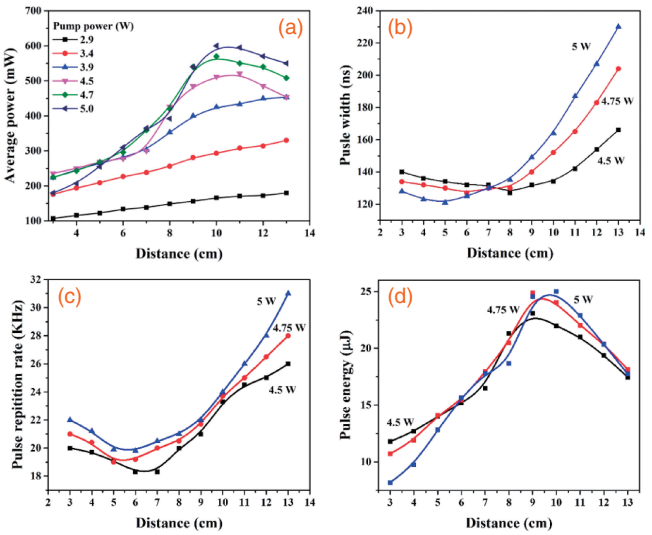

Fig. 3. Influences of distance on (a) average output power, (b) pulse width, (c) pulse repetition rate, (d) pulse peak energy at different pump powers.

to facilitate the description and analyses, these power curves are divided into three regions: the near-M_1 region (the distances from M_1 are 3–4 cm); the center of the cavity (7–8 cm from M_1); and the near-M_2 region (10–13 cm from M_1). There are two stable regions observed in these three regions. For the region near M_2, the first region with stable operation occurs up to about 4.4 W, which is higher than that for the region near M_1. This can be attributed to the changing stability of the laser cavity induced by the TLE in the laser crystal.[26] It can be seen that for the first stable region, the near-M_2 region demonstrates a significantly higher average output power at the same pump condition. The slope efficiency is up to 29.5% without any active cooling, which is about 3 times higher than that of the region near M_1. In contrast to the other two regions, the region near M_2 exhibits the maximum output power, where a rollover in efficiency starts to occur near the pump power of 4.6 W. These results indicate a strong correlation between the average output power and the position of the SA inside the cavity. In addition, low conversion efficiency is observed, which is attributed to the mode mismatch between the pumping beam size and fundamental mode waist.

The SA is usually placed close to M_2 to achieve better laser performance due to the TLE of the laser crystal. Hence, in the case of pump power less than 3.9 W, longer distances produce higher average output power, which is in agreement with the theory. However, for the region near M_2, when the pump power exceeds 4.0 W, an inverse phenomenon occurs, whereby longer distances produce lower average output power. To further investigate this phenomenon, the influence of distance on average output power at different pump powers is measured and shown in Fig. 3(a). It shows that when the pump power is below 3.4 W, the average output power (black and red curves) increases linearly with distance. As the pump power increases, the relation between average power and distance becomes nonlinear, whereby beyond 4.5 W, the average power increases to a maximum value before decreasing. These experimental results show that an optimal distance exists that gives the maximum average output power. This optimal distance is strongly dependent on pump power. When the pump power is 4.5 W, the optimal distance is about 11 cm, and when the pump power is 5.0 W, the optimal distance decreases to about 10 cm. Therefore, this optimal distance to achieve high output power becomes closer to M_1 with increasing pump power.

The effect of position on pulse characteristics is investigated by the measuring pulse width and pulse repetition rate as they vary with distance, as illustrated in Figs. 3(b) and 3(c), respectively. As the distance from M_1 increases, the pulse width and pulse repetition rate slowly decrease before rapidly increasing. There is a crucial factor causing the pulse width and pulse repetition rate to have an inverse relationship, which is the oscillation beam size inside the SA.[16,27] A small beam size results in high optical power density, which easily bleaches the SA crystal, thereby obtaining a long pulse width and high repetition rate.[21] At short distances (<7 cm), the pulse width increases with decreasing pump power. With increasing distance (>7 cm), the pulse width increases with increasing pump power, which is a result of a decrease of the oscillating beam size with increasing distance. Furthermore, the pulse peak energy is calculated and shown in Fig. 3(d). There is a similar trend to that of the average output power [Fig. 3(a)] but the maximum shifts due to the change of the pulse repetition rate. The peak energies at distances of 3 and 10 cm are 8.2 and 25.0 μJ, respectively, which demonstrate about 3 times improvement with a pump power of 5.0 W.

The results establish the effect of the TLE on the optimal distance from M_1 and pump power. The TLE can be explained by calculation with some assumptions made. The pump beam should be located within the Nd:YVO_4 laser crystal, close to the pump surface to achieve high efficiency and output power. The laser crystal can be represented by a thin convex lens located next to the pump surface. The thermal lens focus length is described as[25]

$$f = \frac{\pi K_c \omega_p^2}{P_h(dn/dT)}\left[\frac{1}{1-\exp(-\alpha l)}\right], \quad (1)$$

where K_c is the heat conductivity, ω_p is the pump waist, dn/dT is the temperature-dependent coefficient of the index of refraction, α is the absorption coefficient, and l is the length of the laser crystal. P_h is the fraction of pump power that results in heating. Based on our calculations, for a laser crystal, the pump power that is converted to heat is around 24%, which is determined by the Stokes loss. For a Nd:YVO_4

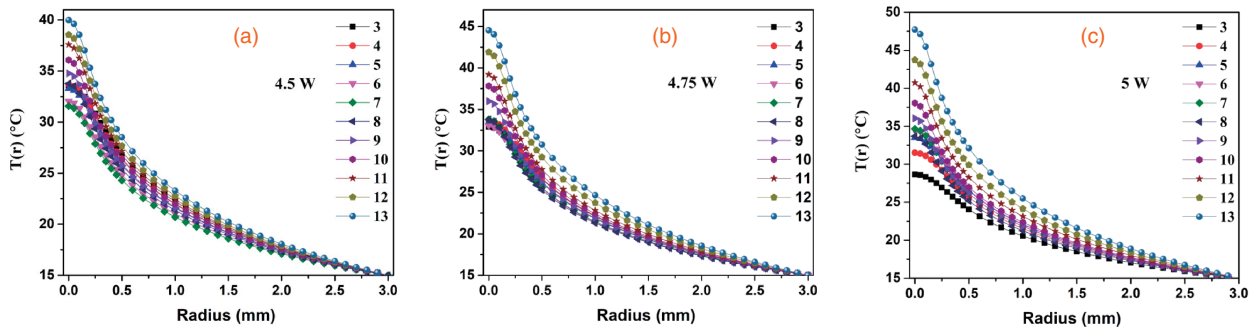

Fig. 4. Temperature distribution of $T(r)$ as a function of r at different distances from M_1 for the input powers of 4.5 W (a), 4.75 W (b), and 5 W (c).

crystal doped with 0.5 at. % Nd^{3+} ions, $K_c = 0.054$ W cm^{-1} K^{-1}, $dn/dT = 4.7 \times 10^{-6}$/K, and $\alpha = 14.8$ cm^{-1}.[15]

Compared to the case of an active crystal, the TLE of the SA inside the cavity is more complex, since the absorption coefficient α is dependent on the intensity of saturation. The temperature distribution $T(r)$ can be obtained from the heat conduction equation. Here, the assumption is that the heat is only removed to the holder with a diameter of 3 mm. Thus, the heat conduction equation can be written as[23]

$$\frac{1}{r}\frac{\partial}{\partial r}\left[r\frac{\partial T(r)}{\partial r}\right] = -\frac{Q(r)}{K_c}, \tag{2}$$

where K_c is the heat conductivity of the SA and $Q(r)$ is the heat generation. Because the oscillating light passes through the SA from two directions inside the cavity, $Q(r)$ should be expressed as

$$Q(r) = \frac{2f(1-T_0)}{L}\int_{-\infty}^{+\infty}\frac{\alpha(r,t)}{\alpha_0}I(r,t)\,dt, \tag{3}$$

where $\alpha(r,t)$ and $I(r,t)$ are respectively the absorption coefficient and the intensity of the propagating beam, which are obtained by[23]

$$\alpha(r,t) = \frac{\alpha_0}{1+\delta_s(t)\exp[-2(r/\omega)^2]}, \tag{4}$$

$$I(r,t) = \frac{2P_p(t)}{\pi\omega^2}\exp[-2(r/\omega)^2], \tag{5}$$

where $\delta_s(t)$ is the saturation parameter and $P_p(t)$ is the time-dependent power, whose expressions are obtained from Ref. 15. In calculations, the parameters of $K_c = 0.12$ W cm^{-1} K^{-1}, $dn/dT = 9.8 \times 10^{-6}$/K are used. The fluorescence lifetime τ_f is selected as 3 μs due to it being a function of temperature and decreasing as the temperature increases. For a single pulse beam, the pulse shape can be approximated as the hyperbolic secant function, which can be written as[23]

$$P_p(t) = \frac{S_p P_{av}\eta}{t_w f T_{oc}}\,\mathrm{sech}\left(S_p\pi\frac{t}{t_w}\right), \tag{6}$$

where P_{av} is the average power, t_w is the pulse duration, and T_{oc} is the transmission of the output coupler. These parameters are selected from the pulse characteristics measured in an experiment. $S_p = 0.84$ is a constant that describes the pulse shape.[28] It is worth noting that the fractional heat-load parameter η is 75% due to the Stokes loss.

Figure 4 shows the temperature distribution of $T(r)$ as a function of r at different distances from M_1. A reasonable phenomenon is observed that the temperature decreases gradually from the center to the edge of the SA. A higher temperature roughly occurs at positions close to M_2. These temperature distribution curves are fitted with a polynomial, which can be expressed as $T(r) = T_1(0) + T_2 r^2$. Since the oscillating beam waist is approximately 0.2 mm, we only fit the central part of the SA, and the focal length of the thermal lens can be obtained by

$$\frac{1}{f_T} = -L\frac{\partial^2 T}{\partial^2 r^2}\frac{dn}{dT}. \tag{7}$$

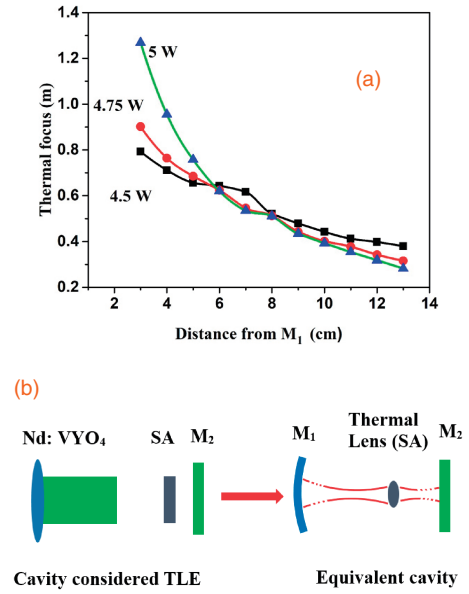

Fig. 5. (a) Thermal focal length versus pump power at different pump beam sizes. (b) An equivalent cavity with the TLE.

Total thermal effects can be made equivalent to a concave lens by combining both an end pump and a crystal thermal effect. The thermal lenses in the SA versus distance from M_1 are calculated for input powers of 4.5, 4.75, and 5 W. It can be seen from Fig. 5(a) that the thermal focal length of the SA decreases as distance increases. The thermal focal length at 4.5 W is shorter than that at the other two input values up to a distance of 6 cm. It is attributed to the higher average power and longer pulse width, which are measured in the experiment and shown in Fig. 3. When the distance is more than 6 cm, the shortest thermal focal length occurs at the highest input power. Figure 5(b) shows that the plane-plane resonator changes to concave-plane resonator. The radius of curvature decreases with increasing thermal lens focal length. For the SA, the thermal lens effect is caused by oscillating light, which is equivalent to a convex lens located inside the cavity.

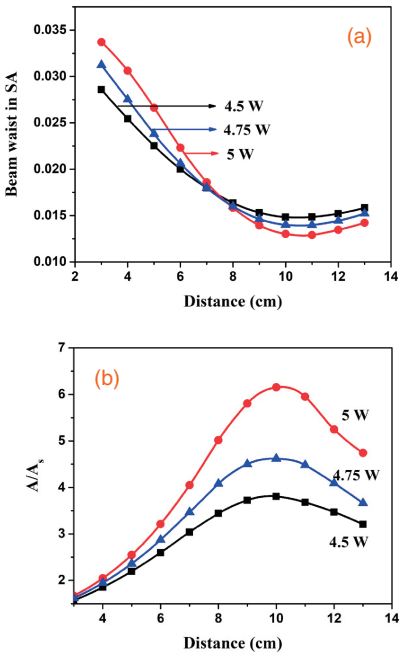

Fig. 6. Calculation results for the beam waist in the SA (a) and the ratio A/A_s (b) as a function of distance at different pump powers.

Therefore, our cavity can be equivalent to a concave-plane resonator with a thin convex lens. Based on an equivalent model, the ABCD transfer matrix and the general stability G-parameters are employed to calculate several equations for cavity parameters. The spot sizes on the surfaces of the laser crystal and SA can be obtained from the equations as[29)]

$$\omega_1^2 = \frac{\lambda L_e}{\pi}\left[\frac{G_2^*}{G_2^*(1-G_1^*G_2^*)}\right]^{1/2}, \tag{8}$$

$$\omega_{SA}^2 = \omega_1^2\left[\left(1-\frac{d_1}{R_1}\right)^2 + \left(\frac{\lambda d_1}{\pi\omega_1^2}\right)^2\right], \tag{9}$$

where λ is the emission wavelength of 1064 nm and the two parameters G_1 and G_2 can be written as

$$G_1^* = \xi - \frac{L_e}{R_1} - Dd_2, \tag{10}$$

$$G_2^* = \xi - \frac{L_e}{R_2} - Dd_1, \tag{11}$$

where d_1 and d_2 represent the distances from M_1 and M_2, respectively, and are shown in Fig. 4(b). D is the focal power and can be expressed as $1/f_T$, where f_T is the thermal lens focal length of the SA. Parameter ξ is given by $(1\text{-}Dl/n)^{0.5}$. L_e is the equivalent cavity length, which is given by

$$L_e = \xi(d_1+d_2) + \frac{l}{n} - Dd_1d_2, \tag{12}$$

where l is the SA length and n is the reflective index of the SA. Because the SA can be equivalent to a thin lens, the beam waist for both sides is approximately equal.

The beam waist size in the SA is an important factor which affects the Q-switching threshold and pulse performance of a passively Q-switched laser. Figure 6(a) shows the calculation results for the beam waist in the SA at different pump powers. As the distance increases, the beam size in SA reduces rapidly and then increases slightly. This can be used to explain the trends of the pulse width [Fig. 3(b)] and pulse repetition rate [Fig. 3(c)], as both have inverse relationships with the beam waist size. According to the definition of beam quality (M^2), the calculated M^2 is about 1.20 when the input power is 5 W. We expect that M^2 can be improved by changing the SA position.

Another important parameter is the ratio A/A_s between the effective area in the gain medium and that in the saturable absorber, which affects the peak energy through α in rate equations with the SA.[21,30)] In this calculation, the ratio has been obtained from the expression $(\omega_1/\omega_{SA})^2$. The dependence on distance at different pump powers is shown in Fig. 6(b). It can be seen that as the pump power increases, the positions of these peaks shift to slightly smaller values that are closer to the M_2 region, which corresponds to Fig. 3(d). When the pump power decreases, the peak value drops. A high value of A/A_s leads to high average output power and peak energy,[21)] and minimization of the oscillating beam inside the SA will achieve the lowest Q-switching threshold. Therefore, the position of the peak corresponds to the highest average output power, which is in agreement with the above measurements. The calculation also highlights the influence of the SA position on A/A_s in the case of high pump power. This is because higher pump power results in more heat accumulation in the laser crystal, the thermal lens focal length reduces, and thus, the radius of curvature becomes smaller. In addition, the intensity of oscillating light increases with the pump power. This results in a shorter thermal focal length and larger focal power for the equivalent lens of the SA. It is worth noting that the position of the peak is unrelated to the smallest size of the oscillating beam in the cavity. Based on the theory of geometrical optics, two focal points might form at both sides of the SA.

In summary, we demonstrate an improvement of the output performance of an end-pumped passively Q-switched Nd:YVO_4 laser by taking advantage of the TLE. In our experiment, a laser crystal and saturable absorber are represented by two optical lenses, which results in a plane-plane resonator changing to a concave-plane resonator with a convex lens. Hence, by optimizing the position of the SA in the laser cavity, the highest average output power and peak energy are observed. We achieve a roughly fourfold increase for the average output power, and the peak energy increases from 8.2 to 25 μJ at the pump power of 5.0 W. We present an equivalent model to explain these experimental phenomena by inducing the TLE. which are in agreement with experimental results. Our results have the potential for the development of compact and low-cost laser techniques.

Acknowledgments This research is supported by the National Research Foundation, Prime Minister's Office, Singapore under its Competitive Research Programme (CRP Award No. NRF-CRP15-2015-04) and administered by National University of Singapore.

1) D. Lin and W. A. Clarkson, Opt. Lett. **42**, 2910 (2017).
2) Q. Yin, H. Lu, and K. Peng, Opt. Express **23**, 4981 (2015).
3) J. Rong, E. Xing, Y. Zhang, L. Wang, S. Shu, S. Tian, C. Tong, X. Chai, Y. Xu, H. Ni, Z. Nui, and L. Wang, Opt. Express **24**, 7246 (2016).
4) H. Yu, H. Liu, G. Ye, S. Fan, Y. Shi, L. Yin, B. Chen, and W. Jiang, Appl. Phys. Lett. **111**, 113507 (2017).
5) H. Liu, H. Yu, W. Jiang, X. Li, S. Fan, B. Lei, Y. Shi, L. Yin, and B. Chen, Sens. Actuators A **251**, 75 (2016).
6) M. Malinauskas, A. Žukauskas, S. Hasegawa, Y. Hayasaki, V. Mizeikis, R.

Buividas, and S. Juodkazis, Light: Sci. Appl. **5**, e16133 (2016).
7) L. Jiang, A. Wang, B. Li, T. Cui, and Y. Lu, Light: Sci. Appl. **7**, 17134 (2018).
8) T. Zhao, W. Jiang, D. Nui, H. Liu, B. Chen, Y. Shi, L. Yin, and B. Lu, Appl. Energy **195**, 754 (2017).
9) T. Dai, Y. Ju, X. Duan, Y. Shen, B. Yao, and Y. Wang, Appl. Phys. Express **5**, 082702 (2012).
10) H. Yu, Z. Wang, H. Zhang, J. Wang, S. Zhuang, and X. Xu, Appl. Phys. Express **4**, 102701 (2011).
11) K. Schuhmann, K. Kirch, F. Nez, R. Pohl, and A. Antognini, Appl. Opt. **55**, 9022 (2016).
12) H. Sakai, H. Kan, and T. Taira, Opt. Express **16**, 19891 (2008).
13) J. Dong, K. Ued, and P. Yang, Opt. Express **17**, 16980 (2009).
14) H. Hong, L. Huang, Q. Liu, P. Yan, and M. Gong, Appl. Opt. **51**, 323 (2012).
15) F. Song, C. Zhang, X. Ding, J. Xu, G. Zhang, M. Leigh, and N. Peyghambarian, Appl. Phys. Lett. **81**, 2145 (2002).
16) R. Bhandari and T. Taira, Opt. Express **19**, 19135 (2011).
17) H. Sakai, A. Sone, H. Kan, and T. Taira, Ext. Abstr. Advanced Solid-State Photonics Tech. Dig., 2006, p. MD2.
18) H. Sakai, H. Kan, and T. Taira, U.S. Patent 7664148 B2 (2010).
19) A. K. Cousins, IEEE J. Quantum Electron. **28**, 1057 (1992).
20) B. Neuenschwander, R. Weber, and H. P. Weber, IEEE J. Quantum Electron. **31**, 1082 (1995).
21) Y.-F. Chen and S. W. Tsai, IEEE J. Quantum Electron. **37**, 580 (2001).
22) J. Y. Huang, H. C. Liang, K. W. Su, and Y. F. Chen, Opt. Express **15**, 473 (2007).
23) J. Song, C. Li, and K. Ueda, Opt. Commun. **177**, 307 (2000).
24) V. A. Kir'yanov and C. G. Bermudez, J. Opt. Soc. Am. B **20**, 2454 (2003).
25) M. E. Innocenzi, H. T. Yura, C. L. Fincher, and R. A. Fields, Appl. Phys. Lett. **56**, 1831 (1990).
26) A. Minassian, B. Thompson, and M. J. Damzen, Opt. Commun. **245**, 295 (2005).
27) J. J. Degnan, IEEE J. Quantum Electron. **31**, 1890 (1995).
28) J. J. Zayhowski and P. L. Kelley, IEEE J. Quantum Electron. **27**, 2220 (1991).
29) J. Xia and M. H. Lee, Appl. Opt. **41**, 453 (2002).
30) G. Xiao and M. Bass, IEEE J. Quantum Electron. **33**, 41 (1997).